Angular Momentum Analysis of Spacecraft with Control Moment Gyros

H. Leeghim
Dept. of Aerospace Engineering, Chosun University
Gwangju 61452, Republic of Korea
h.leeghim@controla.re.kr

ABSTRACT

In this paper, a fundamental approach to analyzing the maneuverability of spacecraft with mounted control moment gyros is addressed by searching feasible angular momentum. The geometrical array of control moment gyros considered is a roof array also known as a 2-SPEED system. Due to the simplicity of the singularity envelope of the array considered, it is reasonably practical to conduct rotational performance analysis of the spacecraft. This maneuverability analysis technique uses a unique chart developed in this work, which allows a guaranteed maximum torque output and angular momentum at any time without concern about the singularity problem of the control moment gyros. Therefore, the purpose of this paper is to provide a conservative method for maneuverability analysis of a spacecraft with installed control moment gyros by searching allowable maximum angular momentum. This method is demonstrated using an illustrative example.

KEYWORDS: *Angular Momentum Analysis,Roof Array, Two-Parallel Single-Gimbal Control Moment Gyros.*

1 INTRODUCTION

The capability of the control moment gyros to generate control torque is significantly greater than provided by reaction wheels of the same power. The higher capability of torque generation, however, has a cost: there is a certain direction in which no control torque can be produced. The singularity problems of the devices make developers hesitate to apply control moment gyros (CMGs) as primary actuators for spacecraft attitude maneuvers. This principal difficulty in employing CMGs is a well-known geometric singularity problem. To overcome this issue, many researchers have been focused on the steering logic of CMG assemblies to avoid the geometrical singularity efficiently [1, 2]. Some representative techniques include the well-known singularity robustness inverse algorithm[3]and the singularity avoidance steering law by null motion[4]. Furthermore, the optimal control technique was introduced into the steering law by minimizing the singularity index and gimbal angular rates simultaneously[5]. It has been proven that the optimal steering law is the generalized form combined both of the singularity robustness inverse algorithm and the steering law by null motion.However, the singularity robustness algorithm always involves torque errors in producing the torque command to avoid the geometrical singularity. The drawback of the steering logic by null motion is that it cannot escape the elliptic singularity due to the little or no existence of null space. For actual applications, it is undesirable to introduce control torque errors and to enter the elliptic singularity. Consequently, no encounter with singularity is better than managing the singularity with robust steering laws.

Limitations related to the geometrical singularity have caused some researchers to focus on the singularity itself[6]. At first, the singular surface concept was invented by defining a unit singular vector. The internal and external singularities connected with the total amount of angular momentum of a CMG array were examined. The elliptic and hyperbolic singularity concepts corresponding to the existence of null spaces used to avoid or escape the singularity were introduced. The Binet-Cauchy identity technique has been used to determine all possible singular gimbal angles[7].Due to the visualization of singular surfaces, many notations were derived about how to avoid or escape the geometrical singularity.

There remains a great deal of effort being directed toward solving the singularity problem while using CMGs as primary actuators for a high agility spacecraft[8,9]. One of the primary reasons not having solved the singularity problem already, might be that maneuverability analysis of a spacecraft with CMGs installed is quite difficult while analysis of rotational maneuverability by reaction wheels is trivial. Even though maneuverability analysis of a spacecraft before flight is mandatory, there is very little analytical and practical information dealing with maneuverability analysis in the literature. Using CMGs of proper size is an important task for spacecraft attitude control system designers to meet the requirement for rapid rotational maneuverability because CMGs are very expensive. Steering an array of CMGs is a difficult task, and little practical approach to determine the maneuverability of such a spacecraft is provided in the literature[10,11]. Thus, offering a practical singularity-free maneuverability analysis method for a spacecraft with CMGs installed is the major motivation for this work.

From a practical point of view, the configuration of the CMG assembly examined in this work is a roof array known as a 2-SPEED(Two Scissored Pair Ensemble, Explicit Distribution) system. This is important because this platform has different characteristics for singular surfaces. This means that roof array have singular surfaces, where it is much easier to avoid singularity when compared to the pyramid array. This property will be reviewed shortly in the next section. The hardware parameters of CMGs, such as the maximum gimbal rates, maximum torque, and maximum angular momentum will also be considered. A new finding for the agility performance analysis presented in this paper is establishing a feasible angular momentum chart of the CMG array, augmented with the singular surface and hardware limits. By inspecting the proposed angular momentum chart with respect to a specified control torque, a guaranteed safe zone can be constructed in which the singularity does not occur and the CMG parameters do not meet or exceed the hardware limits. In other words, the safe zone can be interpreted as the allowable maximum angular momentum envelope. Consequently, it is possible to specify an allowable angular momentum with the developed chart for each axis at all times without any concern for the singularity problem. Therefore, once the parameters required for the performance analysis are obtained, the same method used for conventional reaction wheel assemblies can be employed directly to evaluate the rotational agility of a spacecraft using the CMG array. This approach will dramatically reduce the computational burdens in selecting very suitable CMGs for an initial 'spacecraft attitude control system design' to meet the requirement for high rotational maneuverability.

2 SINGULAR SURFACES OF VARIOUS CMG ARRAYS

Let us examine a few representative array ofsingle-gimbal CMGs useful for understanding the characteristics of the singularity.

2.1 Pyramid Array

The well-known representative array of CMGs for three-axis attitude control systems of a spacecraft is the pyramid configuration depicted in Fig. 1

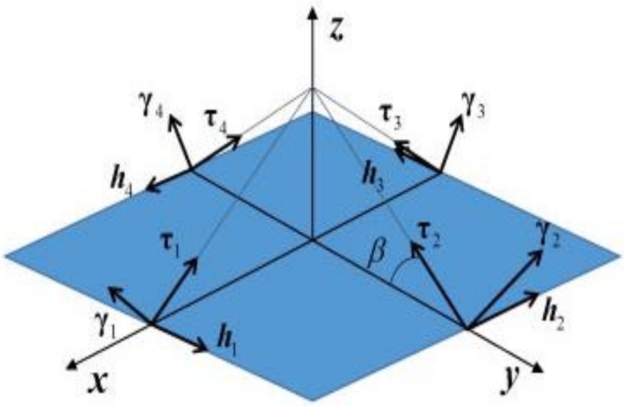

Figure 1: Pyramid array of four single-gimbal CMGs

where $\gamma_i \in \mathrm{R}^3$ and $h_i \in \mathrm{R}^3$ are the gimbal vector and angular momentum vector of *i*-th CMG, respectively.Then, the total angular momentum vector of the CMG system is described as

$$\boldsymbol{h} = \begin{bmatrix} -h_1\cos\beta\sin\gamma_1 - h_2\cos\gamma_2 + h_3\cos\beta\sin\gamma_3 + h_4\cos\gamma_4 \\ h_1\cos\gamma_1 - h_2\cos\beta\sin\gamma_2 - h_3\cos\gamma_3 + h_4\cos\beta\sin\gamma_4 \\ h_1\sin\beta\sin\gamma_1 + h_2\sin\beta\sin\gamma_2 + h_3\sin\beta\sin\gamma_3 + h_4\sin\beta\sin\gamma_4 \end{bmatrix} \quad (1)$$

where γ_i, h_i denote the gimbal angle and magnitude of the angular momentum of i-th CMG, respectively. Note that the magnitude of each angular momentum vector is in general identical from a practical point of view. Now, let us assume that the capacity of angular momentum of the four CMGs is equal without loss of generality such that $h_i = h$.

Next, by differentiating the angular momentum vectors in Eq. 1, the three-axis torque vector can be obtained in matrix form as

$$\boldsymbol{\tau} = A(\boldsymbol{\gamma})\dot{\boldsymbol{\gamma}} \quad (2)$$

where $\dot{\gamma} = [\dot{\gamma}_1, \dot{\gamma}_2, \dot{\gamma}_3, \dot{\gamma}_4]^T \in \mathrm{R}^4$ is the gimbal angular rate vector, and $A \in \mathrm{R}^{3\times 4}$ is the Jacobian matrix defined as

$$\begin{aligned} A(\boldsymbol{\gamma}) &= \frac{d\boldsymbol{h}}{d\boldsymbol{\gamma}} \equiv [\boldsymbol{\tau}_1, \boldsymbol{\tau}_2, \boldsymbol{\tau}_3\boldsymbol{\tau}_4] \\ &= h\begin{bmatrix} -\cos\beta\cos\gamma_1 & \sin\gamma_2 & \cos\beta\cos\gamma_3 & -\sin\gamma_4 \\ -\sin\gamma_1 & -\cos\beta\cos\gamma_2 & \sin\gamma_3 & \cos\beta\cos\gamma_4 \\ \sin\beta\cos\gamma_1 & \sin\beta\cos\gamma_2 & \sin\beta\cos\gamma_3 & \sin\beta\cos\gamma_4 \end{bmatrix} \end{aligned} \quad (3)$$

where $\boldsymbol{\tau}_i$ represents the torque vector generated by the i-th CMG.

2.2 Roof Array

Let us examine the special case of pyramid arrays with the skew angle of $\pi/2$. This is the 2-SPEED single-gimbal CMG systems employed by Crenshaw[12]. Because this array has two orthogonal pairs of two parallel single-gimbal CMGs, it is also called a Roof Array configuration due to its geometrical shape, as illustrated in Fig. 2.

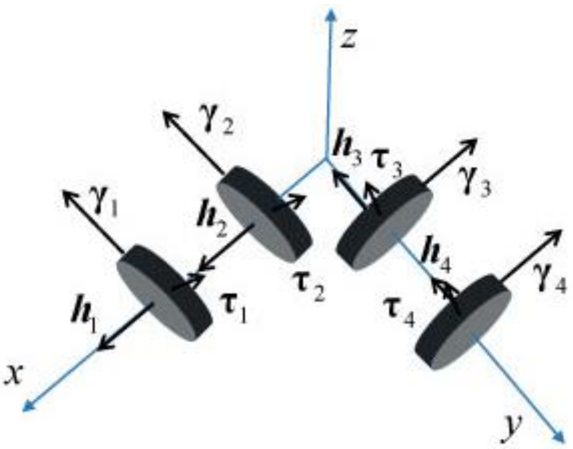

Figure 2: Roof array configuration

The angular momentum vector for this configuration is given simply by

$$\boldsymbol{h} = h\begin{bmatrix} -\cos\gamma_2 + \cos\gamma_4 \\ \cos\gamma_1 + \cos\gamma_3 \\ \sin\gamma_1 + \sin\gamma_2 + \sin\gamma_3 + \sin\gamma_4 \end{bmatrix} \qquad (4)$$

and the corresponding Jacobian matrix is expressed as

$$A(\boldsymbol{\gamma}) = h\begin{bmatrix} 0 & \sin\gamma_2 & 0 & -\sin\gamma_4 \\ -\sin\gamma_1 & 0 & \sin\gamma_3 & 0 \\ \cos\gamma_1 & \cos\gamma_2 & \cos\gamma_3 & \cos\gamma_4 \end{bmatrix} \qquad (5)$$

Next, the two-parallel single-gimbal CMG configurations depicted in Fig. 3 are also of practical importance.

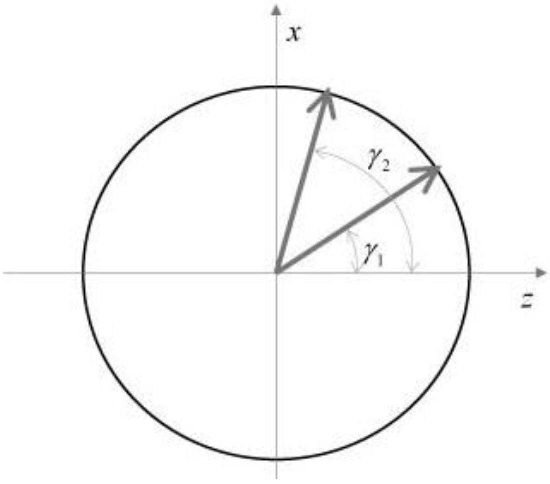

Figure 3: Two-parallel single-gimbal CMG configurations

The total angular momentum vector of this array in matrix form is also given by

$$\boldsymbol{h} = h\begin{bmatrix} \cos\gamma_1 + \cos\gamma_2 \\ \sin\gamma_1 + \sin\gamma_2 \end{bmatrix} \qquad (6)$$

and the Jacobian matrix $A \in \mathrm{R}^{2\times 2}$ is defined as

$$A(\gamma) = h\begin{bmatrix} -\sin\gamma_1 & -\sin\gamma_2 \\ \cos\gamma_1 & \cos\gamma_2 \end{bmatrix} \qquad (7)$$

3 TWO-PARALLEL SINGLE-GIMBAL CMG CONFIGURATIONS

As described in the previous section, the roof array consists of two orthogonal sets of the two-parallel single-gimbal control moment gyroscopes (TPCMGs). Each TPCMG can produce 2-axis control torque. For complete three-axis torque generation, one of the two TPCMGs, for example, has to produce control torque along the *x* and *z*-axes while the other must produce torque for the *y* and *z*-axes. In this case, the capacity of the angular momentum and torque along the *z*-axis can be twice by the two TPCMGs.

Note that $\gamma_1 = \gamma_2 \pm \pi$ is an internal singularity, while $\gamma_1 = \gamma_2$ is a saturation singularity. The corresponding singular vector of the TPCMGs illustrated in Fig. 4 can be the zero-angular momentum vector (internal singularity) where two CMGs are aligned in opposite directions, or the 2h angular momentum vector (external singularity) where two CMGs are aligned in the same direction. Note that no redundancy exists as there are two CMGs for the two-axis torque generation.

Using Eq. 7 the gimbal angular rate vector for a torque command is simply expressed as

$$\dot{\boldsymbol{\gamma}} = A(\gamma)^{-1}\boldsymbol{\tau}_c \qquad (8)$$

From this equation the gimbal rate vector is computed uniquely, meanwhile for the pyramid configuration it is imperative to use the pseudo-inverse algorithm.

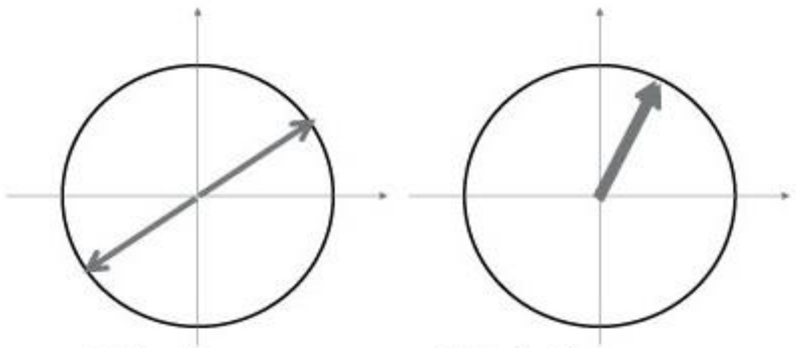

a) 0*h* singularity b) 2*h* singulairty

Figure 4: The singular condition of two-parallel single-gimbal CMGs

3.1 Single-axis Torque Generation

The importance of Eq. 8 is that the gimbal rate can be uniquely mapped through gimbal angles for a specified torque command. In this simulation, the maximum gimbal rate was limited to 1.0 rad/s with the angular momentum of 1 Nms. Thus, the maximum torque output is 1.0 Nm in this case. It is obvious from the numerical simulation results displayed in Fig. 5 that for arbitrary chosen initial gimbal angles, the continuous single-axis torque generation can be successively accomplished until the CMGs enter the 0h or2h singular condition. To meet the continuous torque command exactly near the singularity, it is imperative to speed up the gimbal rate; however, it is not possible to generate the additional continuous torque due to the hardware limit. The determinant of the Jacobian matrix is also depicted in Fig. 5. It is a very reasonable and important property that the angular momentum of x or z-axis remains constant while the single z or x-direction torque command is conducted. Meanwhile, the angular momentum in the coincidence axis for the torque command varies until the CMG pairs fall into the singularity.

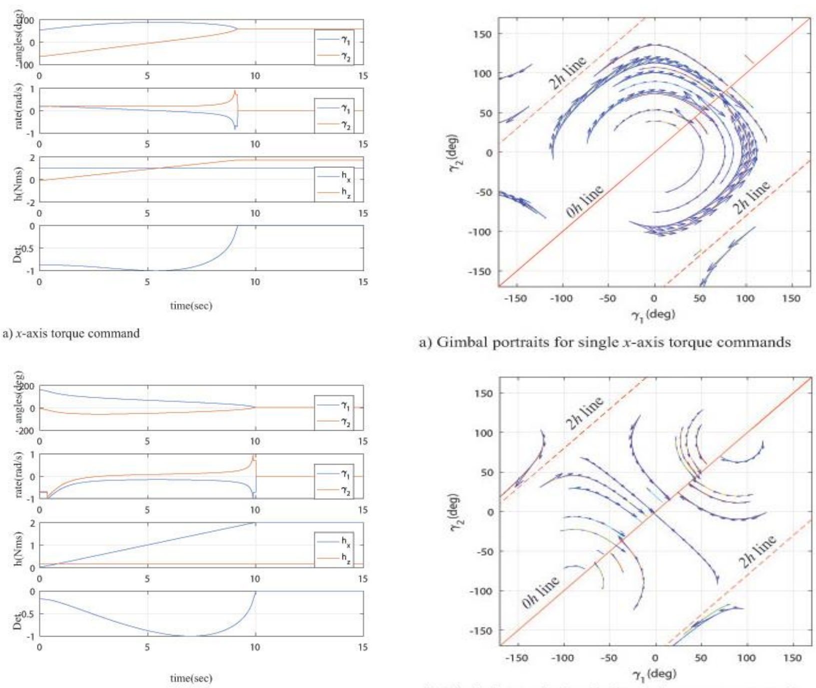

a) *x*-axis torque command a) Gimbal portraits for single *x*-axis torque commands

b) *z*-axis torque command b) Gimbal portraits for single *z*-axis torque commands

Figure 5:Constant torque generation example of TPCMGs for x and y-axis, respectively.

Figure 6: Portrait of the gimbal angular rates for constant torque generation by TPCMGs

3.2 Analysis by Gimbal Spaces

Now, the gimbal angular rate vector needs to be further investigated in gimbal spaces. For randomly chosen initial gimbal angles of (γ_1, γ_2), a few simulations were performed again to produce single-axis constant torque. The portraits of the angular rate vectors in gimbal spaces are plotted in Fig. 6. Note that the slanted centerline is relevant to the 2h singularity of TPCMGs since $\gamma_1 = \gamma_2$, while the dotted lines corresponding to $\gamma_1 = \gamma_2 \pm 180^\circ$ represents the 0h singularity. It is discernible that the singular lines mapped by gimbal spaces are much more easily identified than the singular circles mapped by angular momentum spaces in the previous section. The magnitude of the arrows displayed represent the angular speed of the gimbals at that position to conduct torque generation without errors. The approach to the singular lines coincides with determinant of the Jacobian matrix going to zero. As seen from Fig. 6, an interesting revelation shows that there exist different patterns of gimbal angular rate vectors that might produce the single-axis torque generation along x or z-axis direction. All the trajectories finally end meeting at one point on the singular line with their unique trajectories not crossing the curves at all. This phenomenon leads to the same outcomes illustrated by the examples in Fig. 6.

To show concretely why each gimbal migrates along the distinguished trajectory, let us put the trajectories in Fig. 6 on the angular momentum contour. The resulting overlay of the figures is illustrated in Fig. 7. The trajectories for z or x-axis torque commands are exactly in tune with the constant curve of x or z-axis angular momentum, respectively. This is very surprising, but very transparent results happen that are seemingly expected from the case studies conducted in the previous section.

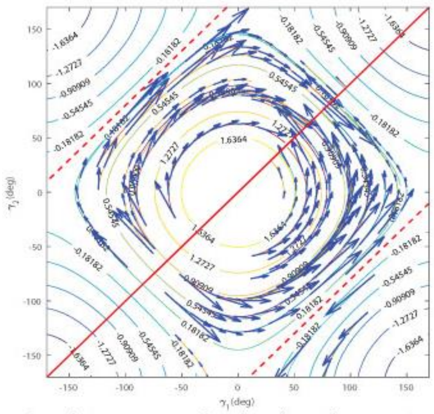

a) *x*-axis torque commands and *z*-axis angular momentum

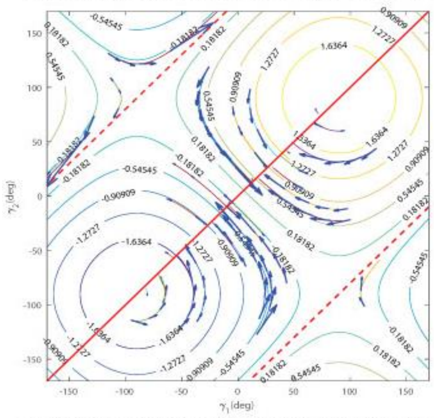

b) *z*-axis torque commands and *x*-axis angular momentum

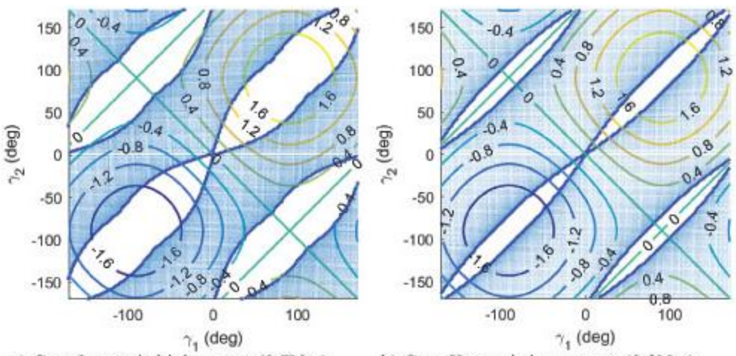

a) Case I : *x*-axis high torque (0.7Nm)

b) Case II: *x*-axis low torque (0.3Nm)

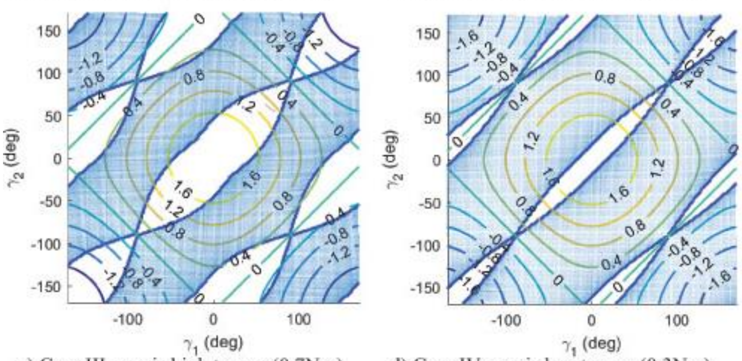

c) Case III: *z*-axis high torque (0.7Nm)

d) Case IV: *z*-axis low torque (0.3Nm)

Figure 7: Overlayed portrait of the angular momentum and gimbal trajectories

Figure 8: Gimbal spaces (blank area) unfeasible to generate a reference torque correctly under the gimbal rate limits

Next, let us define a feasible gimbal space for TPCMGs to conduct a desired torque command exactly under the restricted gimbal angular rates. That is, even if TPCMGs aren't on the singular lines, there is a space in which it is impossible to satisfy the constant torque command without errors due to the hardware limit. The feasible gimbal spaces could be given by using Eq. 8. For a given $\boldsymbol{\tau}_c$ one can evaluate all of the gimbal angular rate vectors as a function of the gimbal angles γ_1 and γ_2. The feasible gimbal space for torque generation can be determined using a simple criterion. That is, the gimbal angles satisfying the condition $\|\dot{\boldsymbol{\gamma}}\|_\infty < \dot{\gamma}_{\max}$ evaluated from Eq. 8 is regarded as the feasible gimbal space, where $\|\cdot\|_\infty$ denotes the infinite norm such that $\|\dot{\boldsymbol{\gamma}}\|_\infty = \max[\dot{\gamma}_1, \dot{\gamma}_2]$ and $\dot{\gamma}_{\max}$ represents the hardware limit of the gimbal rates. Otherwise, the gimbal vector could be treated as belonging to a singular space where the TPCMGs cannot meet the torque command exactly. The resulting infeasible gimbal space, (blank area in the figure), is illustrated in Fig. 8 for a few reference torque values about the x and z-axis. As the level of reference torque is decreased or (increased), the singular space is also reduced or (enlarged).

3.3 Analysis by Gimbal Spaces

For 2-axis rotational agility analysis with hardware limits, let us first define the desired maximum torque vector, $\boldsymbol{\tau}_{\max}$, guaranteed to be produced at all time. The maximum gimbal rate vector which is the hardware limit also needs to be divided into two parts. This division is reserved for each axis to guarantee a certain torque output at all times. By selecting the maximum desired gimbal rate for the x-axis control torque as $\dot{\gamma}_x < \dot{\gamma}_{\max}$, the allowable maximum angular rate remaining for z-axis control torque is constrained as

$$\dot{\gamma}_z = \dot{\gamma}_{\max} - \dot{\gamma}_x \qquad (9)$$

The singular space augmented with the hardware limit of each axis can be determined using the criterion of $\|\dot{\boldsymbol{\gamma}}\|_\infty < \dot{\gamma}_{max}$ by assuming that $\dot{\gamma}_{\max}$ is replaced with ether $\dot{\gamma}_x$ or $\dot{\gamma}_z$.

Putting the angular momentum contours and the singular spaces in one place leads to a feasible angular momentum (FAM) chart uniquely designed for this paper to enable rotational performance analysis of TPCMGs. A representative sample chart is illustrated in Fig. 9. In this case, the angular momentum of the TPCMGs is h = 1.0 (Nms), and the maximum angular rate vector is $\dot{\gamma}_{\max} = 1.0$ (rad/s). Furthermore, $\dot{\gamma}_x$ is also, for instance, chosen as 0.8 (rad/s). The desired maximum torque vector selected is then as $\boldsymbol{\tau}_{\max} = [0.3, 0.075]^T$ (Nm). Consequently, the sample subspace of the feasible gimbal space, enclosed with a bold line in Fig. 9, can be carefully established by attitude control system designers to eliminate the critical singularity problem and to meet the maneuverability requirements, simultaneously.

Note that the enclosed subspace can never meet the singular lines. The allowable angular momentum variation along x-axis direction ranges from about -1.6 (Nms) to about 1.6 (Nms), while along the *z*-axis direction it ranges from about 0.4 (Nms) to about 1.14 (Nms) plotted in the sample chart. Additionally, one of the CMG gimbals γ_1 is allowed to move from about -44° to about 127° while γ_2 ranges from about -127° to about 44°.

Finally, the spacecraft rotational maneuverability provided by a roof array of CMGs could be evaluated by inspecting the two orthogonal sets of TPCMGs. Without loss of generality, the sharing axis of the two TPCMGs discussed in this section is assumed to be the z direction. For convenience, the required agility performance required in both of x and y-axis directions, is assumed to be identical. Thus, inspecting only one TPCMG system in the x-z plane could reveal the performance of the full three-axis rotational maneuverability.

4 CONCLUSIONS

By investigating the singular surfaces for various arrays of four single-gimbal CMGs, it was concluded that the roof array configuration was the best to evaluate the maneuverability performance of a spacecraft due to the simplicity of the singular surfaces. Two-parallel single-gimbal control moment gyro (CMG) systems were also investigated in detail. By using the suggested feasible angular momentum (FAM) chart in gimbal space, it is possible to determine a maximum angular momentum envelope in which the gimbals can freely movable without concern about the singularity problem. Consequently, the desired maximum torque and the allowable maximum angular momentum enable easy analysis of the maneuverability. Of course, the CMGs could provide higher level of performance than the conservative level determined using the FAM chart. Therefore, the technique proposed here could be utilized at a starting point for sizing a CMG or for tuning the attitude control system of a spacecraft employing a roof array of four single-gimbal CMGs.

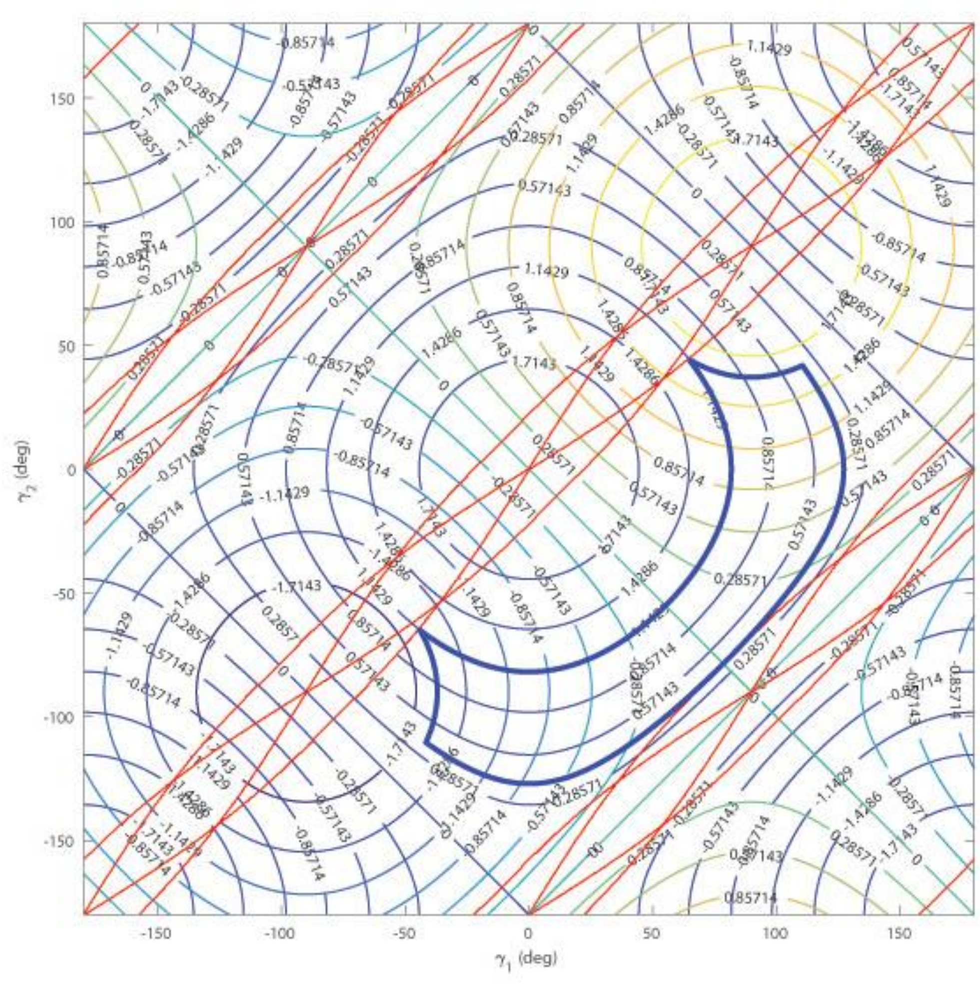

Figure 9: Angular momentum of TPCMG with an optional feasible gimbal subspace to prevent entering into the singular space

REFERENCES

1. B. Wie, Singularity escape/avoidance steering logic for control moment gyro systems, Journal of Guidance, Control, and Dynamics 28 (5) (2005) 948–956.

2. Y. Yao, F. Liu, H. Zhao, Constrained steering law for vscmgs with the function of attitude control and energy storage, Aerospace Science and Technology 58 (2016) 341–350.
3. K. A. Ford, C. D. Hall, Singular direction avoidance steering for control-moment gyros, Journal of Guidance, Control, and Dynamics 23 (4) (2000) 648–656.
4. H. Schaub, J. L. Junkins, Singularity avoidance using null motion and variable-speed control moment gyros, Journal of Guidance, Control, and Dynamics 23 (1) (2000) 11–16.
5. H. Leeghim, H. Bang, J.-O. Park, Singularity avoidance of control moment gyros by one-step ahead singularity index, Acta Astronautica 64 (9) (2009) 935–945.
6. B. Wie, Singularity analysis and visualization for single-gimbal control moment gyro systems, Journal of Guidance, Control, and Dynamics 27 (2) (2004) 271–282.
7. G. Margulies, J. Aubrun, Geometric theory of single-gimbal control moment gyro systems, Journal of the Astronautical Sciences 26 (2) (1978) 159–191.
8. H. Yoon, P. Tsiotras, Spacecraft adaptive attitude and power tracking with variable speed control moment gyroscopes, Journal of Guidance, Control, and Dynamics 25 (6) (2002) 1081–1090.
9. H. Leeghim, I.-H. Lee, D.-H. Lee, H. Bang, J.-O. Park, Singularity avoid- ance of control moment gyros by predicted singularity robustness: ground experiment, IEEE Transactions on Control Systems Technology 17 (4) (2009) 884–891.
10. V. Lappas, W. Steyn, C. Underwood, Attitude control for small satellites using control moment gyros, Acta Astronautica 51 (1) (2002) 101–111.
11. V. Lappas, W. Steyn, C. Underwood, Design and testing of a control moment gyroscope cluster for small satellites, Journal of Spacecraft and Rockets 42 (4) (2005) 729–739.
12. J. Crenshaw, 2-SPEED, a single-gimbal control moment gyro attitude control system, in: AIAA GN&C Conf., Paper 73-895, Key Biscayne, FL, 1973.